Desalination and Water Treatment
www.deswater.com

doi: 10.5004/dwt.2019.23469

140 (2019) 222–230
February

Recovery of magnesium sulfate through crystallization in waste liquid after simultaneous desulfurization and denitrification

Caiduan Zhang[a], Feng Liu[a,*], Haotian Li[a], Xin Qian[a], Fang Zeng[a], Yongliang Ma[b], Lidong Wang[a]

[a]*Department of Environmental Science and Engineering, North China Electric Power University, Baoding, 071003, Hebei, China, Tel. +0086 18903125598; Fax: +0086 3127525533; email: liufeng@ncepu.edu.cn (F. Liu), Tel. +8618833260285; email: ncepuzcd@outlook.com (C. Zhang), Tel. +8618647467218; email: riche.ht@gmail.com (H. Li), Tel. +8615100239317; email: missingfireball@outlook.com (X. Qian), Tel. +8613785436662; email: zf-yy@163.com (F. Zeng), Tel. +86312 7525511; email: wld@ncepu.edu.cn (L. Wang)*
[b]*Department of Environmental Science and Engineering, Tsinghua University, Beijing, 100084, China, Tel. +86 10 62771101; email: liang@tsinghua.edu.cn*

Received 19 June 2018; Accepted 12 November 2018

ABSTRACT

A crystallization scheme for the recovery and reuse of waste liquid after simultaneous desulfurization and denitrification by magnesium oxide/chlorine-based additive was proposed in this paper. Based on the constant-rate cooling crystallization method, the mechanisms of magnesium sulfate crystal formation and growth in the waste liquid were analyzed. Factors such as the solute mass fraction, stirring rate, cooling rate, and final cooling temperature were analyzed to understand their impact on crystal yield, composition, and morphology. The results indicated that supersaturation is the key factor in determining crystal size and form. All of the tested factors have a significant effect on the crystal form. As the initial concentration of solute increases and the final cooling temperature decreases, the spontaneous crystallization yield increases significantly. As the stirring rate and cooling rate increase, the spontaneous crystallization yield slightly decreases.

Keywords: Waste liquid after simultaneous desulfurization and denitrification; Cooling crystallization; Crystal yield; Crystal morphology; Mechanism

1. Introduction

Acid rain and photochemical pollution are serious problems associated with China's air pollution. Currently, haze weather covers a wide area and lasts for a long time, which seriously endangers people's health and limits the sustainable development of the economy and environment [1]. After years of efforts, pollutant emissions from coal-fired power plants, which are the main source of pollution, have been effectively controlled, but air pollution is still intensifying. Therefore, solving the problem of gaseous pollutant emissions from other pollutant sources has become critical to control China's air pollution as the next step.

Coal-fired industrial boilers, represented by iron and steel, petrochemical, smelting, and cement, are the second major source of industrial emissions of atmospheric pollutants in China. According to statistics, there are about 500,000 coal-fired industrial boilers in China, emitting 2.355 million tons of smoke, 6.384 million tons of sulfur dioxide (SO_2), and 7.813 million tons of nitrogen oxides (NO_x), which account for 34.6%, 37.7%, and 13.5%, respectively, of the country's total emissions. Noticeably, the application of desulfurization systems for coal-fired industrial boilers is incomplete, and denitrification control has just started [2]. In addition, there are many constrains in industrial boilers, such as large fluctuations in load, varying operating conditions, strong

* Corresponding author.

corrosive flue gas, small capacity, and weak economic capabilities. Due to the above constrains, the limestone–gypsum desulfurization (WFGD) combined with selective catalytic reduction (SCR) denitrification technology adopted by most power plants is greatly limited when applied to coal-fired industrial boilers, failing to meet the emission requirements of SO_2 and NO_x from coal-fired industrial boilers.

Through the technology of simultaneous desulfurization and denitrification by magnesium oxide (MgO)/chlorine-based additives [3–8], a desulfurization and denitrification efficiency more than 95% can be achieved, showing advantages such as non-fouling, stable operation, low automation, and the integration of absorption and oxidation. This technology is especially suitable for small or medium industrial boilers. However, the waste liquid contains high concentrations of chloride (Cl^-), sulfate (SO_4^{2-}), nitrate (NO_3^-) and magnesium (Mg^{2+}). As the early 1960s, the United States took the lead in studying on recycling technology for waste liquid from desulfurization by MgO, and put forward the method of regenerating MgO and SO_2-rich gas by thickening, separation, drying, calcination and other operations. MgO was returned to the desulfurization system to continue to absorb flue gas, and SO_2 was sent to a sulfuric acid plant to produce acid [9–11]. However, the development of MgO desulfurization technology in China is relatively late, leading to insufficient calcination experience, technical difficulty and high operating cost. Therefore, the waste liquid is often treated by discarding method, double alkali technology (using lime to regenerate $Mg(OH)_2$, the byproduct is gypsum) or magnesium sulfate recovery method [12]. Discharging the waste liquid directly not only causes secondary pollution in the environment but also results in the waste of resources. At the same time, the accumulation of byproduct (gypsum) caused by the double alkali method also leads to serious land occupation problems. Above all, based on the research results of the catalytic oxidation of magnesium sulfite in the previous stage [13–16], a technical solution with unique operation conditions was proposed in this paper to recover Cl^-, SO_4^{2-}, NO_3^- and Mg^{2+} ions from the waste liquid in the form of magnesium salt by a series of operation units such as filtration with impurity removal, evaporation concentration, cooling crystallization, centrifugal separation and drying. The recovered magnesium salt can be used as a raw material for magnesium-based building materials to recycle the byproducts. Through this process, ions in the waste liquid are precipitated in the form of salt, and the content of ion in the discharged waste liquid is greatly reduced, which alleviates the problems of equipment corrosion and secondary pollution. As a key operation unit, the cooling crystallization with the advantages of low energy consumption, safe operation, free of pollution, good selectivity, and high product purity has become the focus of this research [17–20].

Himawan et al. [21] recovered magnesium sulfate heptahydrate ($MgSO_4{\cdot}7H_2O$) through a eutectic cooling crystallization method and found that this method consumed 70% less energy than the triple effect evaporation crystallization method. Compared with the cooling crystallization method, the final temperature needs to be reduced to below 0°C, and the energy consumption is higher. Based on engineering practice, Hu and Li [22] found that it is highly feasible to recover $MgSO_4{\cdot}7H_2O$ from MgO flue gas desulfurization through evaporation, crystallization and drying, showing significant economic and social benefits. Zhang et al. [23] explored the influence of different crystallization conditions on the yield and particle size of $MgSO_4{\cdot}7H_2O$ crystals by single-factor and orthogonal experiments. It was found that the final temperature and the mass fraction of solutes were the main factors affecting the crystallization rate. Ren and Huang [24] found that as the concentration of magnesium chloride ($MgCl_2$) in solution increased, the crystallization temperature and the decomposition temperature of $MgSO_4{\cdot}7H_2O$ increased, the width of the metastable zone first increased and then decreased, and the nucleation stage increased. Other researchers also conducted studies on the effect of different operating conditions and systems on the metastable zone [25–27], supersaturation [28–31] and crystal morphology [32–34].

Although the aforementioned scholars have made many achievements in the field of crystallization research, the crystallization process is complicated, and the yield and morphology of the crystal product are closely related to the system characteristics. Therefore, even for systems with similar properties, the main influencing factors and influence laws will be quite different due to the different interactions between ions. The crystallization of waste liquids after simultaneous desulfurization and denitrification by MgO/chlorine-based additives has not been publicly reported. Here waste liquid after simultaneous desulfurization and denitrification by MgO/chlorine-based additives was studied. Based on the cooling crystallization method, the mechanisms of crystal formation and growth were analyzed. The main factors affecting crystal yield, components and morphology were investigated. This study is an important part in the recovery of waste liquid after simultaneous desulfurization and denitrification by MgO/chlorine-based additives. It provides basic data for the subsequent recovery of ions (Cl^-, NO_3^-) as well as theoretical guidance for the crystallization of $MgSO_4$ in practical engineering applications.

2. Experimental setup

2.1. Experimental methods and apparatus

The experimental set is shown in Fig. 1.

According to the content of the major components in the waste liquid after simultaneous desulfurization and denitrification by the MgO/chlorine-based additive, the experimental solution was prepared by weighing a proper amount of solute with an electronic analytical balance (FA2004 model, precision ± 0.0001 g, Shanghai, China) followed by dissolving in deionized water. The solute in the experiment referred to a mixture of $MgSO_4$, magnesium chloride ($MgCl_2$), and magnesium nitrate ($Mg(NO_3)_2$) at a mass ratio of 6.2:2:1. Unless otherwise specified herein, all reagents were AR grade. The pH of the solution was determined by a pH meter (Raymond Model PHS-3E, Shanghai, China). The prepared solution was transferred to a set of self-designed, double-jacket closed glass crystallizers (S212-2, Jiangsu, China) with an inner layer volume of 2 L for the crystallization reaction. In the course of the reaction, a constant speed stirrer (5GU3KB, 90 W, 50 rpm–750 rpm, Beijing, China) was used to ensure uniform mixing of the solution. The conductivity of the solution and the temperature were monitored in real time by a

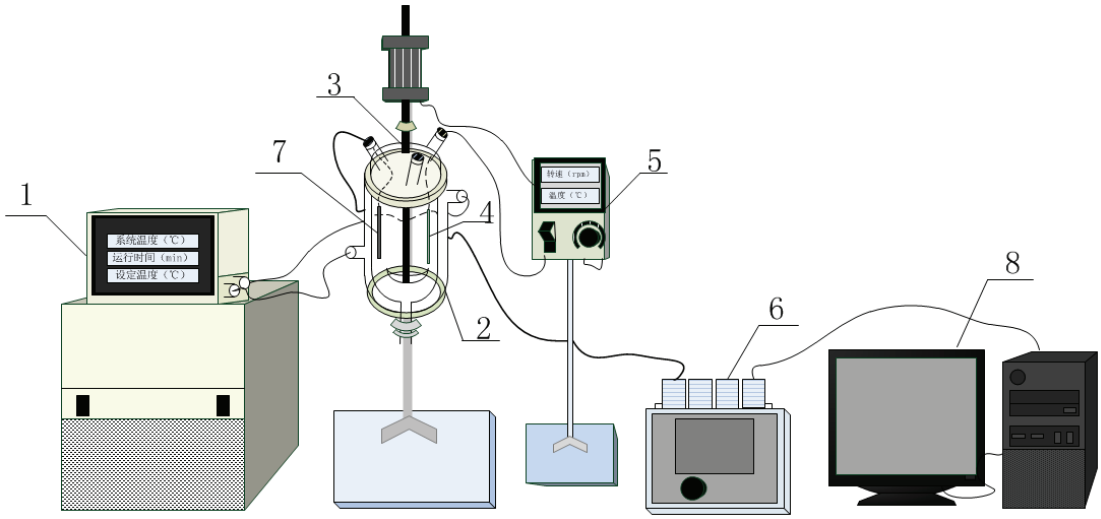

Fig. 1. Experimental setup. 1—Isothermal bath; 2—jacket-type crystallizer; 3—agitator paddle; 4—temperature sensor; 5—constant-speed stirrer; 6—conductivity meter; 7—conductivity electrode; 8—computer.

conductivity meter (Rayfy DDSJ-319L, Shanghai, China). The computer monitored and recorded the initial nucleation conductivity values and temperatures. The cooling and heating process of the solution was precisely controlled by an intelligent energy-saving constant temperature bath (DC-2006, precision ± 0.1°C, Ningbo, China) with dual temperature sensors. At the end of crystallization, crystals were obtained by suction filtration through a circulating water type multipurpose vacuum pump (SHB-111 type, Henan, China) and were dried in an electric heated blast drying box (model 101, Beijing, China) at 45°C to a constant weight.

The composition of the crystalline product was determined by X-ray diffraction (XRD, Bruker D8 Advance, Germany), with a CuKα1 radiation (λ = 0.154056 nm), a scanning rate of 0.1° s^{-1}, and incidence angles of 5°–90° (2θ). The morphology of the crystalline product was characterized by scanning electron microscopy (SEM, Hitachi S-4800, Japan).

2.2. Calculation methods

The equation used to calculate the crystallization yield is shown in Eq. (1):

$$\eta = C'/C \times 100\% \quad (1)$$

where η—crystallization yield (%); C'—weight of the crystal after crystallization (g); C—weight of the initial solute (g).

3. Mechanism of crystal formation and growth

The formation and growth of $MgSO_4$ crystals consist of four stages: formation of supersaturated solution, nucleation, crystal growth, and recrystallization [35], as shown in Fig. 2.

As illustrated in Fig. 2(a), the solution does not undergo crystallization before reaching final supersaturation, and each ion (Mg^{2+}, Cl^-, SO_4^{2-} and NO_3^-) exists in a free state.

With the temperature of the system decreases, the solution gradually approaches critical solubility. Since the mass concentration of $MgSO_4$ in the experimental waste liquid is the largest, and the solubility at the same temperature is the smallest, under the impetus of supersaturation, the nucleus of $MgSO_4$ hydrate is formed first, and the primary heterogeneous nucleation process is completed, as seen in Fig. 2(b). According to kinetics [36], the nucleation rate of the crystal nucleation rate is expressed in Eq. (2) as follows:

$$\gamma_N = dN/dt = K_N \cdot \Delta C^m \quad (2)$$

where N—the total number of particles in solution of unit volume (number of particles/m^3); K_N—nucleation rate constant (number of particles $mol^{-m} \cdot m^{3m-3} \cdot s^{-1}$); m—nucleation order (constant, generally greater than 2); ΔC—supersaturation (°C).

From Eq. (2), it can be seen that the nucleation rate is positively correlated with supersaturation.

After the crystal nucleus particles are formed, the $MgSO_4$ crystal grows continuously around its core, but under the action of stirring, the solute unit constantly moves, causing the crystal to collide with other crystals, the reactor wall, and the stirring paddle to break the $MgSO_4$ crystal. Small crystals less than the critical size are dissolved, increasing the supersaturation of the solution and facilitating the formation and growth of nuclei, as shown in Fig. 2(c).

Undissolved, broken crystals and newly generated nuclei continue to grow as growth cores, and $MgSO_4$ crystals aggregate to form clusters and structurally stable hydrogen bonding networks [37], as shown in Fig. 2(d). Similar to the nucleation rate, the crystal growth rate is also highly correlated with supersaturation. According to the chemical kinetics, the expression of the crystal growth rate γ_G is shown in Eq. (3), indicating that there is a positive correlation between growth rate and supersaturation.

$$\gamma_G = dL/dt = K_G \cdot \Delta C^l \quad (3)$$

where L—size increase of the crystal in a linear direction; K_G—rate constant of crystal growth; l—order of crystal growth (constant, between 1 and 2).

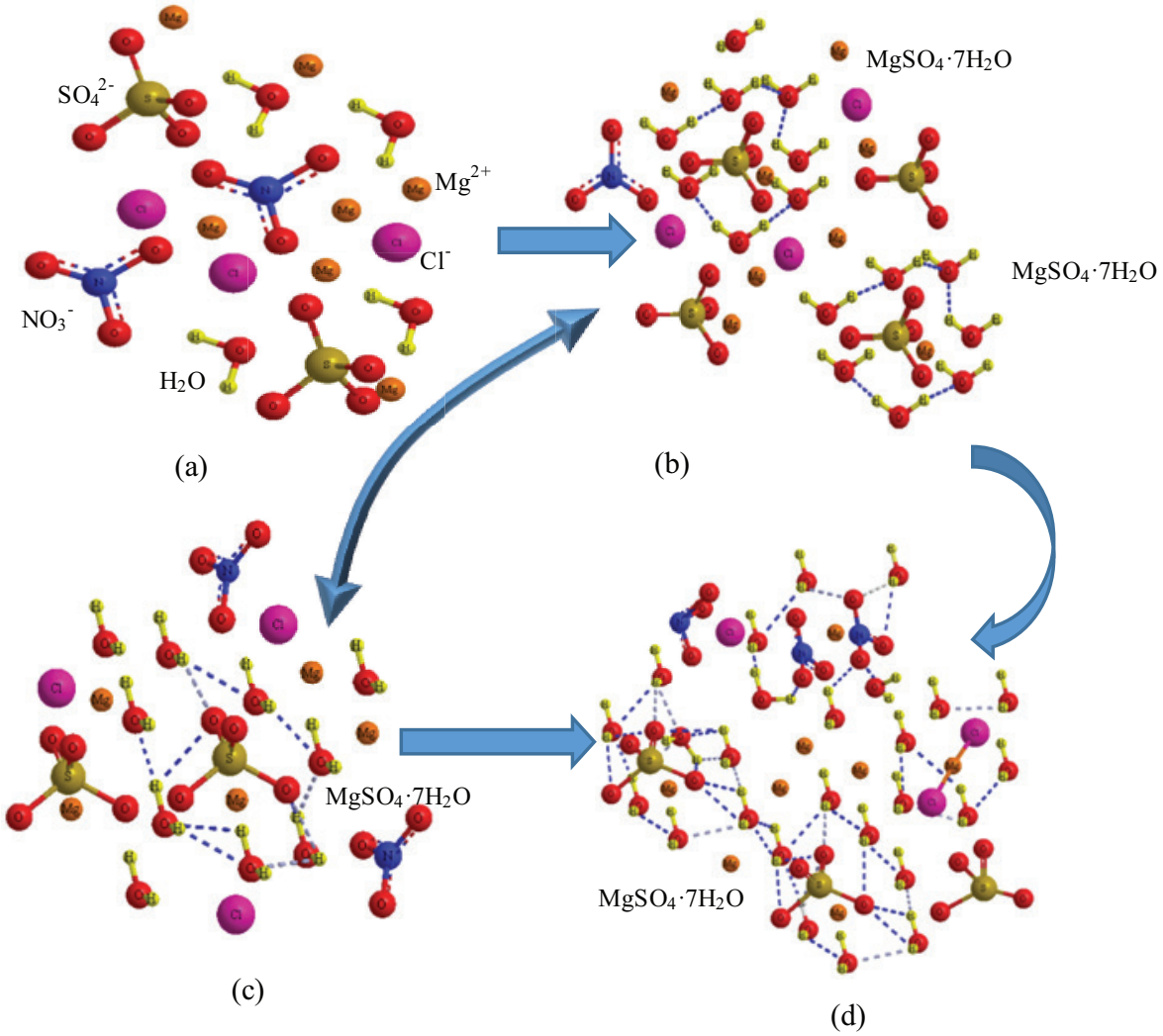

Fig. 2. Formation and growth of $MgSO_4$ crystals. (a) Slurry, (b) nucleus formation, (c) nucleation and dissolution of crystal nuclei, (d) nuclei growth.

The crystallization rate consists of the nucleation rate and growth rate, and both rates are affected by the same factor—supersaturation. Therefore, there is a positive correlation between the nucleation rate and growth rate. Combining Eqs. (2) and (3) gives Eq. (4).

$$\gamma_N/\gamma_G = K_N/K_G \cdot \Delta C^{m-l} \quad (4)$$

From the aforementioned equations, it can be seen that "$m - l$" ≥ 0 and K_N/K_G is a constant. As can be seen from Eq. (4), as the supersaturation "ΔC" increases, the γ_N, γ_G, and γ_N/γ_G increase, but the increase rate of γ_N is greater than that of γ_G. When $\gamma_N > \gamma_G$, the size of the $MgSO_4$ crystal is small, and its crystal form is simple. Conversely, as the supersaturation "ΔC" decrease, the decrease rate of γ_N is greater than that of γ_G, and the crystal growth is the dominant reaction, producing large $MgSO_4$ crystals with a regular shape. Therefore, supersaturation is a key factor affecting particle size and crystal form. In experimental research and engineering practice, it is necessary to pay great attention to the control of supersaturation.

4. Experimental results and analysis

4.1. Effect of initial mass fraction of the solute on crystallization

The initial mass fraction of the solute is directly related to supersaturation, which is an important factor that determines the crystal growth rate and nucleation rate. Therefore, we first examined the effect of the initial mass fraction (wt.) of the solute on crystallization. According to sampling results at industrial sites, the solute mass fraction of the waste liquid before crystallization is 28%–30%, the initial solute mass fraction of 26%–32% was adopted in this experiment. The other experimental parameters were as follows: the stirring rate was 50 rpm, the cooling rate was 8°C/h, the final temperature was 25°C. In order to ensure the reproducibility of experimental data, at least three parallel experiments were carried out for each influential factor. The same method was also adopted in other experiments. The experimental results are shown in Figs. 3–5.

As can be seen from Fig. 3, the waste liquid cannot complete primary nucleation when the wt. is less than 29%. This is because at higher final temperatures and lower

concentrations, the waste liquid has less supersaturation, and the resulting driving force is insufficient for nucleation. In addition, when the temperature is lower than 48°C, the $MgSO_4$ crystals precipitate as the form of $MgSO_4 \cdot 7H_2O$. The high crystallized water content facilitates the formation of a supersaturated solution, making it difficult to produce nuclei [38]. After adding $MgSO_4 \cdot 7H_2O$ seeds (0.0257 g, 200 mesh) to the waste liquid, considerable nucleation was immediately observed. This is because the addition of nuclei significantly reduces the undercooling of crystallization and the nucleation energy barrier.

Above 29% wt., primary nucleation can take place spontaneously, and the crystallization yield increases with increasing wt. This is because with increasing wt., the corresponding saturated temperature of the waste liquid increases, and the higher temperature can not only generate a higher degree of supersaturation but also decrease the width of the metastable zone. As a result, the crystal nucleation rate, growth rate, and crystallization yield also increase. However, at high supersaturation, the crystals are mainly nucleated, which results in a smaller crystal size and a simple crystal form. Comparing Fig. 4 with Fig. 5, it can be seen that when the wt. is increased from 28% to 30%, the crystal form becomes obviously fragmented and the crystal grains are small. Therefore, the control of wt. is particularly important for obtaining suitable supersaturation and crystal products with large grain sizes and simple crystal forms.

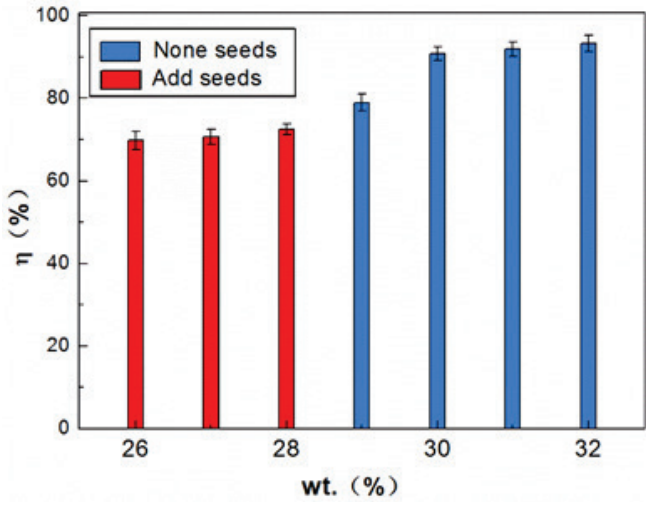

Fig. 3. Effect of initial mass fraction of the solute on crystallization yield.

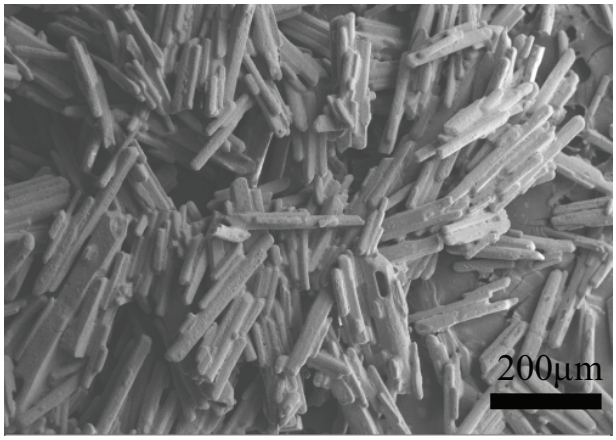

Fig. 4. SEM image of a crystal with an initial mass fraction of the solute of 28%, a stirring rate of 70 rpm and a final temperature of 20°C.

4.2. Effect of stirring rate on crystallization

Stirring increases the deposition rate of solute on the solid surface and is essential in the crystallization process. In this experiment, the influence of the stirring rate on crystallization was explored under experimental conditions with the initial mass fraction of the waste liquid 28%, the cooling rate 5°C/h, the final temperature 20°C, and the stirring rate (*S*) 50–300 rpm. The experimental results are shown in Figs. 6 and 7.

As can be seen from Fig. 6, the waste liquid fails to spontaneously nucleate when the stirring rate is lower than 70 rpm or higher than 300 rpm. Secondary nucleation is completed only after adding seeds. The reason is deduced as follows:

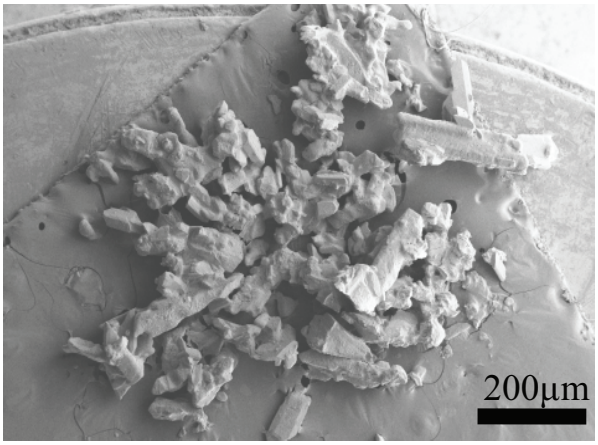

Fig. 5. SEM image of a crystal with an initial mass fraction of solute 30%, a stirring rate of 70 rpm and a final temperature of 20°C.

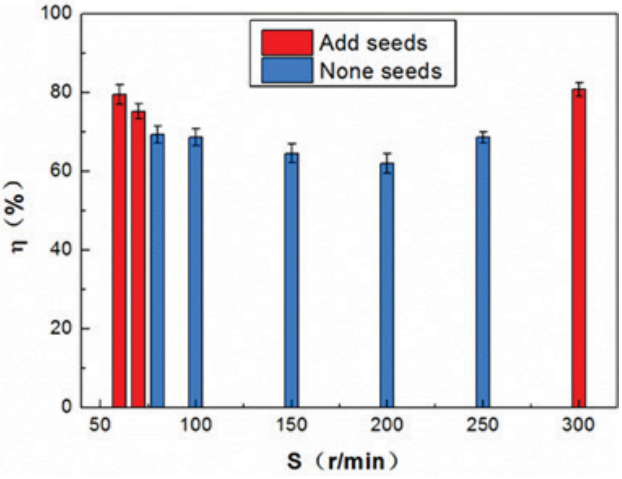

Fig. 6. Effect of the stirring rate on crystallization yield.

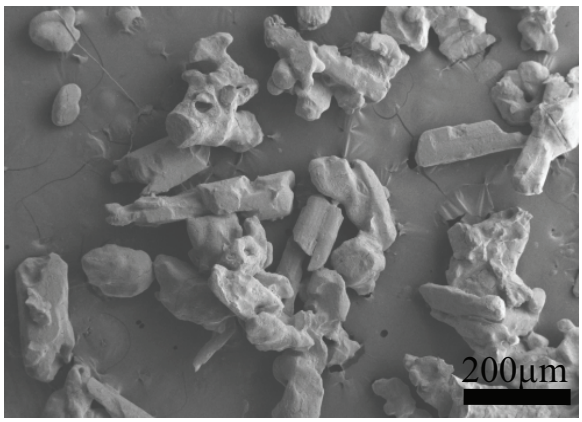

Fig. 7. SEM image of crystal obtained at a stirring rate of 150 rpm.

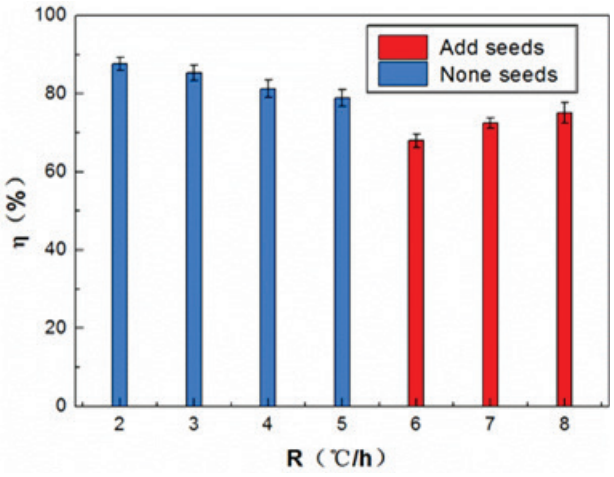

Fig. 8. Effect of the cooling rate on crystallization yield.

the collision probability and energy between the ion-moving units in the liquid phase at low stirring rate are not sufficient to combine with each other to form a linear body, and more difficult to further form crystal nuclei. In contrast, at a high stirring rate, a larger fluid shear force is generated. The force breaks the nucleus into particles which are smaller than the critical size. These particles are completely dissolved and ultimately unable to nucleate. When the stirring speed is between 70 and 300 rpm, primary nucleation takes place in the waste liquid and the crystallization yield maintains stable. This is because a proper stirring rate provides not only a suitable rate of heat and mass transfer in the waste liquid but also enough collision energy of the moving units, avoiding excessive crushing and abrasion of the crystal. Comparing Fig. 4 with Fig. 7, it can be seen that the greater the stirring rate, the more severe the collision of the crystals, which results in a smaller size of the crystal product and wider particle size distribution.

In summary, the stirring rate determines particle size distribution of the product. Under the premise of ensuring waste liquid mixing uniformly, low-speed stirring should be used in the experimental and engineering application process to obtain crystals with good crystal shape, large particle size and uniform particle size.

4.3. Effect of cooling rate on crystallization

Similar to weight, the cooling rate is also an important factor affecting the degree of supersaturation. The experimental parameters were as follows: the initial waste liquid mass fraction was 28%; the stirring rate was 70 rpm; the final temperature was 20°C and the cooling rates (R) were 2°C/h–8°C/h. The experimental results are shown in Figs. 8 and 9.

As can be seen from Fig. 8, when R is below 6°C/h, the initial nucleation occurred spontaneously in the waste liquid. As the cooling rate increases, the crystallization yield decreases slightly. After R reaches 6°C/h, the nucleation requirement cannot be achieved. This is due to the induction period that the solution needs to undergo from supersaturation to nucleation. The greater the cooling rate of the system, the greater the temperature drop during the induction period, which results in a lower temperature that corresponds with the super solubility and the wider metastable zone at the same saturation temperature. Thus, the formation of nuclei becomes less likely. In addition, the viscosity of

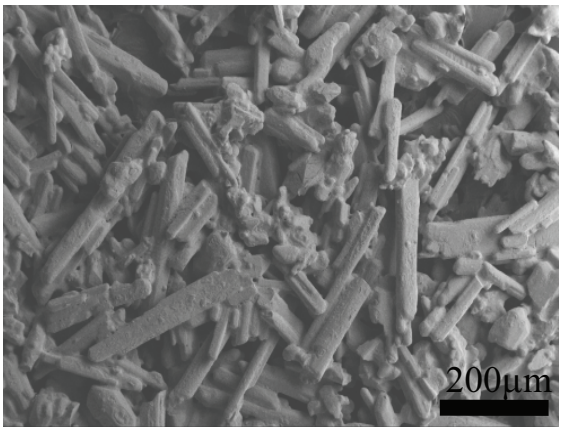

Fig. 9. SEM image of a crystal obtained at a cooling rate of 2°C/h.

the solution changes significantly with temperature. As the nucleation temperature decreases, the viscosity increases and the diffusion rate of the solute to the crystal nucleus slows down; further, the probability of solute collision decreases, decreasing the probability of nucleation. Comparing Fig. 9 with Fig. 4, the grain size of the crystal product is small and non-uniform. This is because when the cooling rate is small, the induction period of the system is prolonged, and the accumulation time of supersaturation is extended, increasing the possibility of spontaneous nucleation. The formation of a large number of nuclei can cause the crushing and abrasion of crystals, thereby reducing the crystal size.

4.4. Effect of final cooling temperature on crystallization

$MgSO_4$ is a substance with positive solubility characteristics, that is, its solubility in water increases with increasing temperature. Therefore, the temperature has a significant effect on the dissolution and crystallization of $MgSO_4$. The nucleation rate constant and growth rate constant of the crystals increase with increasing temperature. Therefore, the effect of the final cooling temperature of the solution on the crystallization process is explored. The final temperature of the solution cooling (T_f) was chosen as 10°C–25°C.

The initial mass concentration was 28%. The stirring rate was 70 rpm. The cooling rate was 5°C/h. The experimental results are shown in Figs. 10 and 11.

As can be seen from Fig. 10, when T_f is below 22°C, primary nucleation is spontaneously completed in the waste liquid. As the final temperature decreases, the yield of the crystals increases, and spontaneous crystallization cannot occur at 22°C or above. This is due to the fact that when the T_f is high, the supersaturation formed after the completion of cooling is insufficient to promote nucleation. As the final temperature decreases, the solubility of the waste liquid decreases, the supersaturation increases, and the nucleus forms readily. The formation of the nucleus, in turn, reduces the total free energy of the system, promotes the precipitation of new nuclei, and improves the crystal yield. As illustrated in Fig. 11, the morphology of the crystal is intact when the T_f is 10°C, but it needs a large amount of energy to decrease the temperature of waste liquid. Considering the economy, productivity, and product quality, it is preferable to use a higher final temperature in practice.

Considering the experiment results, crystal yield and quality, the optimum conditions for crystal formation of $MgSO_4{\cdot}7H_2O$ were determined: initial mass fraction of the solute 28%, stirring rate 70 rpm, cooling rate 5°C/h and final cooling temperature 20°C. Under the optimum conditions, the yield of crystallization reached 80%.

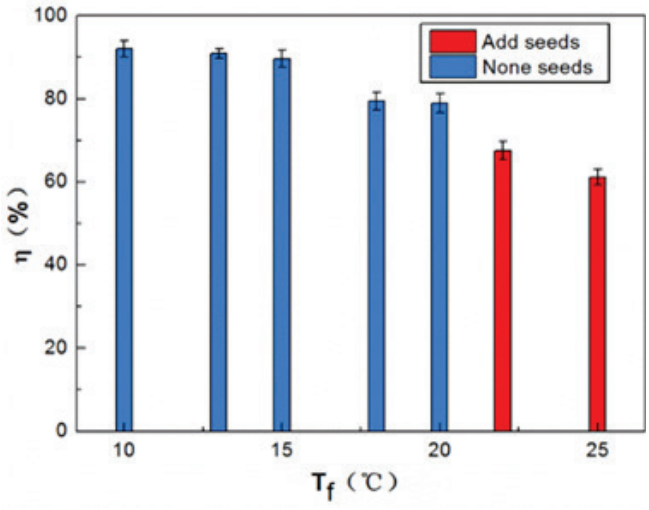

Fig. 10. Effect of final cooling temperature on crystallization yield.

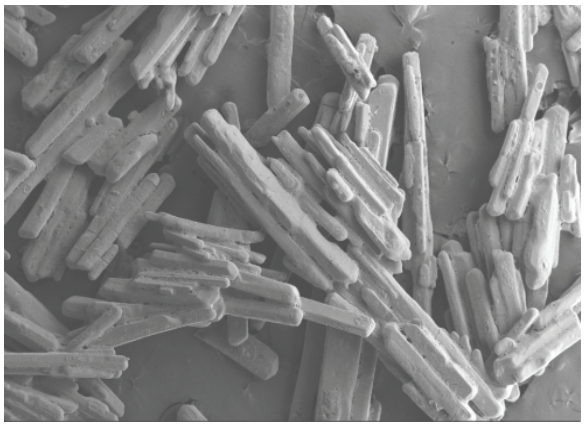

Fig. 11. Crystals obtained under a final cooling temperature of 10°C.

4.5. Composition analysis of crystal

In order to characterize the crystal composition, four groups of representative crystals were selected for XRD analysis. The analysis results are shown in Fig. 12.

The results show that under various conditions, the XRD patterns of the obtained crystal products all correspond to the standard spectrum of $MgSO_4{\cdot}7H_2O$, and no other material peaks were observed. This shows that the operating conditions have no effect on the crystal composition, and the resulting crystalline product is confirmed to be $MgSO_4{\cdot}7H_2O$. Under the optimal experimental conditions, the crystallization rate reaches 80%. Zhang et al. [23] conducted an experimental study on pure magnesium sulfate. According to their experiment results, the crystallization rate was 53% when the mass fraction is 34%. Comparing his findings and the results in this paper, it indirectly shows that the addition of appropriate amounts of magnesium chloride and magnesium nitrate will not only maintain the purity of the crystalline product but also facilitate the precipitation of magnesium sulfate crystals.

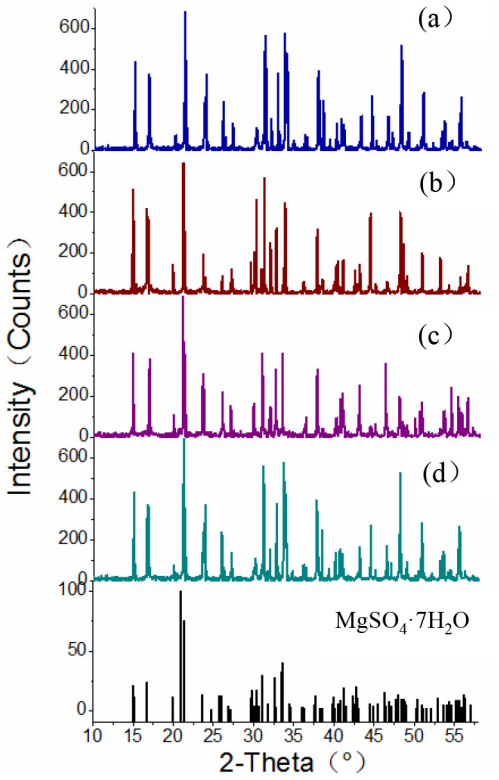

Fig. 12. XRD pattern of a crystal. (a) A solute mass fraction of 32%, stirring speed of 70 rpm, cooling rate of 8°C/h, and final cooling temperature of 20°C; (b) a solute mass fraction of 28%, stirring speed of 70 rpm, cooling rate of 8°C/h, and final cooling temperature of 10°C; (c) a solute mass fraction of 28%, stirring speed of 300 rpm, cooling rate of 8°C/h and final cooling temperature of 20°C; (d) a solute mass fraction of 28%, stirring speed of 70 rpm, cooling rate of 2°C/h and final cooling temperature of 20°C.

5. Conclusion

- According to the characteristic of waste liquid after simultaneous desulfurization and denitrification by MgO/chlorine-based additive, the optimal experimental conditions are determined. Under the optimum conditions, the yield of crystallization reaches 80%, particle size distribution is uniform, and crystal forms are intact.
- In a mixed solution of $MgSO_4$, $Mg(NO_3)_2$, and $MgCl_2$, the crystal obtained by the cooling crystallization method is $MgSO_4·7H_2O$. No other crystals are observed.
- The solute mass fraction, stirring rate, cooling rate and final cooling temperature have significant effects on the crystal size and form. With the increasing of the mass fraction of the solute, the stirring rate, and the cooling rate, and the decreasing of the final cooling temperature, the particle size and crystal form intend to become smaller and simpler, respectively, and vice versa. The initial solute concentration and the final cooling temperature have a significant effect on the spontaneous crystallization yield, while the stirring rate and the cooling rate have little effect.
- The mechanism analysis shows that supersaturation is a key factor that affects crystal size and form. When the degree of supersaturation is high, the size of $MgSO_4·7H_2O$ crystals is small and the crystal form is simple; otherwise, the size of $MgSO_4·7H_2O$ crystals is large and the crystal form is regular.

Acknowledgements

The authors would like to thank the National Natural Science Foundation of China (51508188) and the State Key Research Program (2016YFC0204102) for supporting this study.

References

[1] R.L. Hao, Y. Zhao, B. Yuan, S.H. Zhou, S. Yang, Establishment of a novel advanced oxidation process for economical and effective removal of SO_2 and NO, J. Hazard. Mater., 318 (2016) 224–232.
[2] B. Shen, Y. Han, L. Price, H. Lu, M. Liu, Techno-economic evaluation of strategies for addressing energy and environmental challenges of industrial boilers in China, Energy, 118 (2017) 526–533.
[3] G. Cheng, C.X. Zhang, Desulfurization and Denitrification technologies of coal-fired flue gas, Pol. J. Environ. Stud., 27 (2018) 481–489.
[4] R.L. Hao, S. Yang, B. Yuan, Y. Zhao, Simultaneous desulfurization and denitrification through an integrative process utilizing $NaClO_2/Na_2S_2O_8$, Fuel Process. Technol., 159 (2017) 145–152.
[5] J. Wang, W.Q. Zhong, Simultaneous desulfurization and denitrification of sintering flue gas via composite absorbent, Chin. J. Chem. Eng., 24 (2016) 1104–1111.
[6] R. Del Valle-Zermeño, M. Niubó, J. Formosa, M. Guembe, J.A. Aparicio, J.M. Chimenos, Synergistic effect of the parameters affecting wet flue gas desulfurization using magnesium oxides by-products, Chem. Eng. J., 262 (2015) 268–277.
[7] L.Y. Yan, X.F. Lu, Q. Guo, Q.H. Wang, X.Y. Ji, Research on the thermal decomposition and kinetics of byproducts from MgO wet flue gas desulfurization, Adv. Powder Technol., 25 (2014) 1709–1714.
[8] Z. Shen, X. Chen, M. Tong, S. Guo, M. Ni, J. Lu, Studies on magnesium-based wet flue gas desulfurization process with oxidation inhibition of the byproduct, Fuel, 105 (2013) 578–584.
[9] B.H. Song, Wet magnesium oxide flue gas desulfurization process: a review, China Environ. Prot. Ind., 8 (2009) 28–30.
[10] Q. Guo, A study on magnesia FGD regeneration technology, Nonferrous Metals Eng. Res., 32 (2011) 37–39.
[11] L. Yan, X. Lu, Q. Wang, Y. Kang, J. Xu, Y. Chen, Research on sulfur recovery from the byproducts of magnesia wet flue gas desulfurization, Appl. Therm. Eng., 65 (2014) 487–494.
[12] L. Yan, Research on regenerative cycle and utilization of MgO wet flue gas desulfurization byproducts, Chongqing University, 2014.
[13] T. Zhu, Y. Ma, H. Zhang, D. Li, L. Li, X. Zhou, B. Song, J. Hao, Experimental investigation of $MgSO_3$ oxidation process by catalysis in the magnesium desulfurization, Catal. Today, 258 (2015) 70–74.
[14] T. Qi, L. Wang, S. Wu, Q. Li, J. Liu, L. Meng, H. Xiao, Insight into structural role of 2D/3D mesoporous silicon in catalysis of magnesium sulfite oxidation, Appl. Catal. A, 566 (2018) 33–43.
[15] Q. Li, Y. Yang, L. Wang, P. Xu, Y. Han, Mechanism and kinetics of magnesium sulfite oxidation catalyzed by multiwalled carbon nanotube, Appl. Catal. B, 203 (2017) 851–858.
[16] L. Wang, T. Qi, J. Wang, S. Zhang, H. Xiao, Y. Ma, Uniform dispersion of cobalt nanoparticles over nonporous TiO_2 with low activation energy for magnesium sulfate recovery in a novel magnesia-based desulfurization process, J. Hazard. Mater., 342 (2018) 579–588.
[17] R. Del Valle-Zermeño, J. Formosa, J.A. Aparicio, J.M. Chimenos, Reutilization of low-grade magnesium oxides for flue gas desulfurization during calcination of natural magnesite: a closed-loop process, Chem. Eng. J., 254 (2014) 63–72.
[18] L. Wang, H. Feng, Y. Dong, J. Peng, W. Li, Solubility and metastable zone width of aqueous sodium dichromate dihydrate solutions in the presence of sodium chromate additive, J. Cryst. Growth, 454 (2016) 105–110.
[19] H. Lu, J. Wang, T. Wang, N. Wang, Y. Bao, H. Hao, Crystallization techniques in wastewater treatment: an overview of applications, Chemosphere, 173 (2017) 474–484.
[20] T. Wang, H. Lu, J. Wang, Y. Xiao, Y. Zhou, Y. Bao, H. Hao, Recent progress of continuous crystallization, J. Ind. Eng. Chem., 54 (2017) 14–29.
[21] C. Himawan, H.J.M. Kramer, G.J. Witkamp, Study on the recovery of purified $MgSO_4·7H_2O$ crystals from industrial solution by eutectic freezing, Sep. Purif. Technol., 50 (2006) 240–248.
[22] Q. Hu, Y. Li, The process technology application of magnesium hydrate recovery from magnesium oxide flue gas desulfurization, Chem. Enterprise Manage., (2013) 241.
[23] Y.B. Zhang, Y.M. Chen, Y.L. Ma, Effects of several crystallization conditions on the recovery of desulfurization by-products, Ind. Saf. Environ. Protect., 37 (2011) 32–34.
[24] X.J. Ren, X.L. Huang, Phase equilibria in the quaternary system of $Li^+,Mg^{2+}//Cl^-,SO_4^{2-}$-$H_2O$ at 273.15 K, Inorg. Chem. Ind., 48 (2016) 13–15, 28.
[25] L.-D. Shiau, Comparison of the interfacial energy and pre-exponential factor calculated from the induction time and metastable zone width data based on classical nucleation theory, J. Cryst. Growth, 450 (2016) 50–55.
[26] M. Jin, P. Frohberg, Y. Sun, P. Li, J. Yu, J. Ulrich, Study on metastable zone width and crystal growth of a ternary system: case study $MgCl_2·6H_2O$·1,4-dioxane, Chem. Eng. Sci., 133 (2015) 181–189.
[27] X.X. Sun, Y.Z. Sun, J.G. Yu, Cooling crystallization of aluminum sulfate in pure water, J. Cryst. Growth, 419 (2015) 94–101.
[28] H. Takiyama, Supersaturation operation for quality control of crystalline particles in solution crystallization, Adv. Powder Technol., 23 (2012) 273–278.
[29] N. Sanzida, Z.K. Nagy, Iterative learning control for the systematic design of supersaturation controlled batch cooling crystallisation processes, Comput. Chem. Eng., 59 (2013) 111–121.
[30] A. Borisenko, Nominal vs. actual supersaturation of solutions, J. Cryst. Growth, 486 (2018) 122–125.
[31] Z. Liang, M. Zhang, F. Wu, J.-F. Chen, C. Xue, H. Zhao, Supersaturation controlled morphology and aspect ratio

changes of benzoic acid crystals, Comput. Chem. Eng., 99 (2017) 296–303.
[32] S.Y. Qin, Y.F. Zhang, Y. Zhang, Nucleation and morphology of sodium metaborate dihydrate from NaOH solution, J. Cryst. Growth, 433 (2016) 143–147.
[33] S. Li, J. Xu, G. Luo, Control of crystal morphology through supersaturation ratio and mixing conditions, J. Cryst. Growth, 304 (2007) 219–224.
[34] D. Aquilano, F. Otálora, L. Pastero, J.M. García-Ruiz, Three study cases of growth morphology in minerals: halite, calcite and gypsum, Prog. Cryst. Growth Charact. Mater., 62 (2016) 227–251.
[35] L. Peng, H. Dai, Y. Wu, Y. Peng, X. Lu, A comprehensive review of phosphorus recovery from wastewater by crystallization processes, Chemosphere, 197 (2018) 768–781.
[36] J.J. Jiang, Measurement of Crystallization Metastable Zone and Study on Particle Size Control of Ammonium Perchlorate, Nanjing University of Science and Technology, 2013.
[37] B. Tansel, G. Lunn, O. Monje, Struvite formation and decomposition characteristics for ammonia and phosphorus recovery: a review of magnesium-ammonia-phosphate interactions, Chemosphere, 194 (2018) 504–514.
[38] T.L. Ye, Principle and Application of Chemical Crystallization Process, Beijing University of Technology Press, 2006.